2009

Analysis of the effects of conical indentation variables on the indentation response of elastic-plastic materials through factorial design of experiment

JOURNAL OF MATERIALS RESEARCH, v.24, n.3, p.1222-1234, 2009
http://producao.usp.br/handle/BDPI/14684

Analysis of the effects of conical indentation variables on the indentation response of elastic–plastic materials through factorial design of experiment

Sara Aida Rodríguez Pulecio,[a] María Cristina Moré Farias, and Roberto Martins Souza
Surface Phenomena Laboratory, Department of Mechanical Engineering, University of São Paulo, 05508-900 São Paulo – SP. Brazil

(Received 31 July 2008; accepted 8 December 2008)

In this work, the effects of conical indentation variables on the load–depth indentation curves were analyzed using finite element modeling and dimensional analysis. A factorial design 2^6 was used with the aim of quantifying the effects of the mechanical properties of the indented material and of the indenter geometry. Analysis was based on the input variables Y/E, R/h_{max}, n, θ, E, and h_{max}. The dimensional variables E and h_{max} were used such that each value of dimensionless Y/E was obtained with two different values of E and each value of dimensionless R/h_{max} was obtained with two different h_{max} values. A set of dimensionless functions was defined to analyze the effect of the input variables: $\Pi_1 = P_l/Eh^2$, $\Pi_2 = h_c/h$, $\Pi_3 = H/Y$, $\Pi_4 = S/Eh_{max}$, $\Pi_6 = h_{max}/h_f$, and $\Pi_7 = W_p/W_T$. These six functions were found to depend only on the dimensionless variables studied (Y/E, R/h_{max}, n, θ). Another dimensionless function, $\Pi_5 = \beta$, was not well defined for most of the dimensionless variables and the only variable that provided a significant effect on β was θ. However, β showed a strong dependence on the fraction of the data selected to fit the unloading curve, which means that β is especially susceptible to the error in the calculation of the initial unloading slope.

I. INTRODUCTION

Instrumented indentation test (IIT), frequently called nanoindentation, is today one of the most commonly used techniques to measure mechanical properties of thin films and small volumes. IIT uses high-resolution instrumentation for control and measurement of loads and penetration depths of an indenter, when it is driven into and withdrawn from the studied material, in a cycle of load and unload.[1–3]

Simple but general results of elastic–plastic indentation response, using the concept of self-similarity, have been obtained.[4–11] The basic idea of dimensional analysis is that physical laws do not depend on the arbitrariness in the choice of units of physical quantities. This concept allows reducing the number of parameters describing the physical phenomena, thus making them simpler to obtain, either from calculations or experiments.[10]

The full factorial design is a statistical technique that allows reliable conclusions through a relatively smaller amount of data, obtained from systematic experiments.[12] This useful technique has been used for many experimental materials research[13–16] and it is also appropriate in computational experiments,[17–20] including finite element simulations of a given experimental procedure.[20]

In this work, the effects of conical indentation variables (factors) on the load–depth IIT curves were analyzed using dimensionless analysis and design of experiments. The statistical significance of factor effects was assessed from the comparison of the effect magnitude with the experimental confidence interval and by plotting the effects on normal probability paper.[12] This study aims to contribute with the discussion that exists in the literature regarding the effect of experimental errors on the accuracy of the calculation of mechanical properties from the indentation data.[21] Additionally, this work attempts to analyze if the tip roundness effect[22] is significant when the ratio R/h is low. The use of statistical tools permits these studies, with the advantage of allowing other analyses, such as the joined effect of multiple input variables. The possibility of these second order effects may be obtained through the use of normal plots, as described in the literature.[12]

II. INDENTATION VARIABLES

Figure 1 shows a typical curve of load as a function of penetration depth (P–h) obtained during IIT. The initial unloading slope (S) is defined as dP/dh at the maximum load, P_{max} is the maximum load obtained in the test, h_{max} is the maximum indentation depth, h_f is the residual indentation depth after complete unloading, $W_T = W_e + W_p$ is the work done by load P during the loading cycle, W_p is the stored (plastic) work after the

[a]Address all correspondence to this author.
e-mail: sara.pulecio@poli.usp.br
DOI: 10.1557/JMR.2009.0124

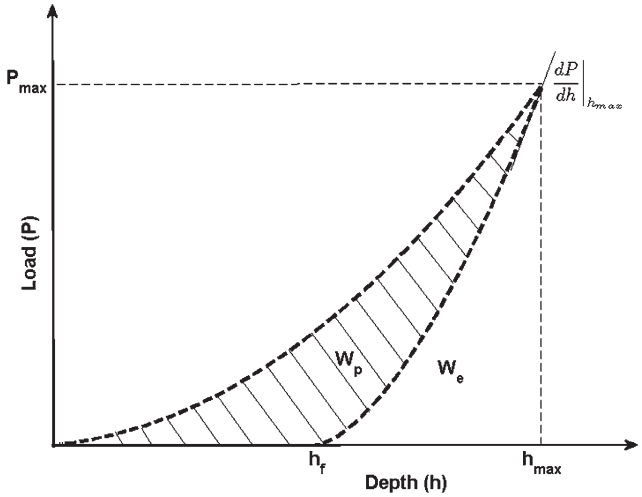

FIG. 1. Schematic illustration of a typical *P–h* response of an elasto–plastic material to instrumented sharp indentation.

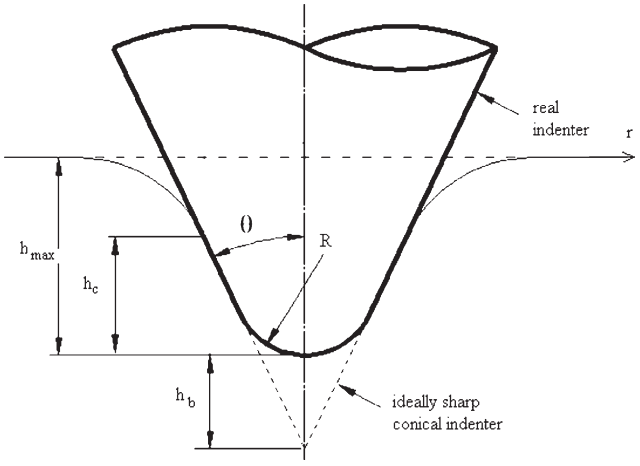

FIG. 2. Illustration of ideally sharp conical indenter and that with a spherical tip.

complete unloading and W_e is the area under the unloading curve, which corresponds to the elastic work recovery of the material.

During the loading stage, the load (P_l) follows the relation[23]:

$$P_l = Ch^{\alpha} \quad , \tag{1}$$

where exponent α is equal to 2 for a conical indenter with perfect shape (no tip roundness[23]) and 3/2 for spherical indenters,[23,24] and C is a coefficient that indicates the curvature of the *P–h* loading curve.

During unloading, the *P–h* curve follows the relation[25]:

$$P_u = K(h_{max} - h_f)^m \quad , \tag{2}$$

where K is the curvature of the unload curve; m is the exponent of the curve and P_u is the load during the unloading stage.

Hardness (H) is defined [Eq. (3)] as the maximum indentation load (P_{max}) divided by the contact area (A_c).[26]

$$H = \frac{P_{max}}{A_c} \quad . \tag{3}$$

The initial unloading slope (S) may be related to the reduced elastic modulus (E_r) through Eq. (4),[23] where β is a correction factor, which is dependent on both indenter geometry and Poisson's coefficient.[27–29] Other works have shown dependence of β with the indentation size when the indenter tip presents some roundness[5,30–33] and with the indenter elastic deformation.[34]

$$E_r = \frac{\sqrt{\pi}}{2\beta}\frac{S}{\sqrt{A_c}} \quad . \tag{4}$$

The reduced elastic modulus is defined as Eq. (5), where E_i and ν_i are the elastic modulus and Poisson's ratio of the indenter, respectively, and E and ν are the elastic modulus and Poisson's ratio of the indented material, respectively.

$$\frac{1}{E_r} = \frac{(1-\nu^2)}{E} + \frac{(1-\nu_i^2)}{E_i} \quad . \tag{5}$$

In experimental indentation tests, the reduced modulus is calculated from Eq. (4) and the elastic modulus is calculated by solving Eq. (5) for E. In this research, the indenter was modeled as rigid, such that the term considering the properties of the indenter was equal to zero. Since E and ν are known input variables in the simulation, E_r was calculated from Eq. (5) and Eq. (4) was used to calculate β, considering the values of S and A_c obtained directly from the finite element simulations.

III. DIMENSIONAL ANALYSIS

In the dimensional analyses, P_l is commonly considered as a function of h, ν, E, ν_i, and E_i,[34] as well as (i) two other mechanical properties of the indented material: initial yield stress (Y) and strain hardening exponent (n)[10]; (ii) friction coefficient (μ)[35]; (iii) indenter geometry (Fig. 2): tip radius (R)[4,22] and semiapex angle (θ)[10]; and (iv) level of residual stresses in the specimen.[36] In this work, the indented material was considered free of residual stresses and the values of the Poisson's ratio and friction coefficient were fixed, being equal to 0.3 and 0.15, respectively. Additionally, the elastic deformation of the indenter was not considered, because it was simulated as rigid. Note that the use of reduced elastic modulus reduces the errors of this simplification[37] when experimental test curves are analyzed using results obtained with rigid indenters. Besides, a consistent analysis on the error in assuming a rigid indenter for the study of the indentation of elastic–plastic cases was not found in the literature. However, for

perfectly elastic and superhard materials the error in elastic modulus calculation was quantified to be from −5–8%, depending on the ratio E/E_i.[34]

Without considering the constant variables, the indentation load during the loading stage was written as indicated in Eq. (6):

$$P_l = f(h, E, Y, n, R, \theta) \quad . \tag{6}$$

Applying the Π theorem of the dimensional analysis,[10] Eq. (6) becomes

$$P_l = Eh^2 \Pi_1 \left(\frac{Y}{E}, \frac{R}{h}, n, \theta \right) \quad , \tag{7}$$

where Π_1 is a dimensionless function, $\Pi_1 = P_l/Eh^2$. This equation indicates that [coherent with Eq. (1)] the load is not proportional to the square of the penetration depth, when R is different from zero, since P_l is dependent of R/h. It is important to mention that literature provides other length parameters (L) (h/L,[10] h/R^4) for this equation.

Following the same idea, the ratio h_c/h, ratio H/Y, S, factor β, ratio h_{max}/h_f, and ratio W_p/W_T can be respectively expressed through Eqs. (8)–(13). Further details on dimensional analysis can be found in Ref. 10:

$$\frac{h_c}{h} = \Pi_2 \left(\frac{Y}{E}, \frac{R}{h}, n, \theta \right) \quad , \tag{8}$$

$$\frac{H}{Y} = \Pi_3 \left(\frac{Y}{E}, \frac{R}{h}, n, \theta \right) \quad , \tag{9}$$

$$S = \left. \frac{dP_u}{dh} \right|_{h=h_{max}} = Eh_{max} \Pi_4 \left(\frac{Y}{E}, n, \frac{R}{h_{max}}, \theta \right) \quad , \tag{10}$$

$$\beta = \Pi_5 \left(\frac{Y}{E}, n, \frac{R}{h_{max}}, \theta \right) \quad , \tag{11}$$

$$\frac{h_{max}}{h_f} = \Pi_6 \left(\frac{Y}{E}, \frac{R}{h_f}, n, \theta \right) \quad , \tag{12}$$

$$\frac{W_p}{W_T} = \Pi_7 \left(\frac{Y}{E}, \frac{R}{h_{max}}, n, \theta \right) \quad . \tag{13}$$

Hence, the instrumented indentation test is described by the dimensionless functions: $\Pi_1 = P_l/Eh^2$, $\Pi_2 = h_c/h$, $\Pi_3 = H/Y$, $\Pi_4 = S/Eh_{max}$, $\Pi_5 = \beta$, $\Pi_6 = h_{max}/h_f$, and $\Pi_7 = W_p/W_T$. The dimensionless function for factor β [Eq. (11)] can be obtained from the combination of Eqs. (4), (8), and (10), which is coherent with previous works.[5]

IV. FACTORIAL DESIGN OF EXPERIMENT

Experiment designs[12] are well-developed methodologies that apply statistics in a way of developing a plan of experiments, which minimize the effort for a desired reliable result. In the design of experiments, it is supposed that the system is composed of a group of independent input variables (factors), and the results for each configuration, which are the outputs (response). A class of designs of great practical importance is the two-level factorial design (mathematically represented by 2^{N12}). To conduct this kind of design, a fixed number of values (or levels/versions) are selected for each one of the factors and then experiments are run with all possible combinations of the factors.

For the case of the instrumented indentation analysis presented in this work, the factors were Y/E, n, R/h_{max}, and θ, which have their physical meaning. The variables Y/E and n are mechanical properties, where Y/E is the strain from which the indented material deformation is no longer elastic and n is the strain-hardening exponent of the indented material. The parameters R/h_{max} and θ are geometric factors that indicate the tip roundness level relative to the indentation depth and semiapex angle, respectively.

Besides the dimensionless factors Y/E, n, R/h_{max}, and θ, two factors were also selected: E and h_{max}. Therefore, each value of the factor Y/E was obtained with two different values of E and each value of the factor R/h_{max} was obtained with two different h_{max} values. Since there are two levels ($a = 2$) for each of the six factors ($N = 6$) of the present approach, the complete arrangement is a $a_1 \; x \; a_2 \; x \; \ldots \; a_N = 2^6$ factorial design. Table I shows the two levels defined for each of the factors analyzed in this work for the 2^6 full factorial design, for which 64 different conditions (or runs) are required.

In terms of the responses, simulation data was used to calculate the following indentation outputs: the load exponent α and dimensionless functions $\Pi_1 = P_l/Eh^2$, $\Pi_2 = h_c/h$, $\Pi_3 = H/Y$, $\Pi_4 = S/Eh_{max}$, $\Pi_5 = \beta$, $\Pi_6 = h_{max}/h_f$, and $\Pi_7 = W_p/W_T$.

The objective of a two-level factorial design is to estimate the effect of the factors on the response, which can be not only due to the individual effect of each factor (mean effect, l_i), but also due to the result of the interaction between two or more factors (interactive effects). In general terms, the effect of a factor is defined as the change in the response as the levels of the factor change (from its low to its high level). The mean effect of a factor is a measurement of the average effect of this factor over all combinations of the levels of the other factors (or conditions/runs). When the effect of a factor 1 is different at the two levels of a factor 2, it is said that the two factors interact. In this case, the interaction effect is defined as half of the difference between the

TABLE I. Layout of designed experiment.

Factors	Y/E	R/h_{max}	n	θ	E (GPa)	h_{max} (μm)
Level low (−1)	0.0013	0.6605	0.16	66.5°	119.929	0.8552
Level high (+1)	0.0039	1.3898	0.34	73.5°	240.071	1.4530

TABLE II. Data for a 2^2 factorial design, example for calculation of effects.

	Variable R/h_{max}		Variable θ		
Run	Original unit of variable	Code unit of variable	Original unit of variable	Code unit of variable	Response $\Pi_1=P_1/Eh^2$
1	0.7018	−1	66.5	−1	0.1595
2	1.4036	1	66.5	−1	0.1804
3	0.7018	−1	73.5	1	0.2847
4	1.4036	1	73.5	1	0.3018

average effect of factor 1 with the upper level of factor 2 and the average effect of factor 1 with the lower level of factor 2.[12]

To further explain the previous concepts, Table II presents a 2^2 factorial design, in which the factors are R/h_{max} and θ and the response is the dimensionless function Π_1. The response values in Table II were obtained maintaining the factors Y/E, n, E, and h_{max} constant and at the low level.

In Table II the value of Π_1 in experiment 1 and 2 differ only because of the ratio R/h_{max}; the semiapex angle of the indenter (θ) is the same. In total there are two measures of the R/h_{max} effect at each of the two levels of factor θ. The individual measure of the effect of changing the R/h_{max} ratio from 0.7018 to 1.4036 is 0.1804–0.1595 = 0.0209 and 0.3018–0.2847 = 0.0171. The average of these two measures (0.019 in this case) is called the main effect of R/h_{max} ratio $l_{R/h}$= 0.019. Because of the symmetry of the design, there is a similar set of two measures for the effect of θ and in each one the level of the remaining factor is constant. In the 2^2 factorial design of Table II the effect of R/h_{max} is larger with θ equal to 66.5 (0.0209) than with θ equal to 73.5 (0.0171). In this case, the factors R/h_{max} and θ are said to interact. A measure of this interaction is given by the difference between the R/h_{max} effect with θ equal to 66.5 and the R/h_{max} effect with θ equal to 73.5 (0.0209–0.0171 = 0.0038). By convention the half of this difference is called the R/h_{max} by θ interaction $l_{R/h\times\theta}$ = 0.0019.

The statistical significance of factor effects is assessed from the comparison of the effect magnitude with the experimental confidence interval or by plotting the effects on normal probability paper.[12] The statistical analysis of effects by normal probability plots is often more efficient and is based on the concepts of the cumulative distribution.[12] In this case, the effects (both main and interactions effects) are supposed to be a random sample taken from a roughly normal distribution with population mean equal to zero. Each effect (i = 1,2,..., M) is associated with the intercept of the cumulative distribution [P_i = 100(i-1/2) M]. Hence, the normal plot of effects is obtained by plotting the probability P_i (in log scale) versus the effects values. Effects with magnitudes close to zero fit on the straight line of the normal plot, which means that they can be considered as noise. Therefore, the effects outside the straight line are statistically significant.[12]

V. FINITE ELEMENT ANALYSIS

A finite element analysis, using the commercial software ABAQUS (Providence, RI), was carried out to simulate the indentation response of elastic–plastic solids. The indenter was considered as a rigid two-dimensional (2D) cone with a rounded tip.

The tested material was represented by 2D mesh of 37,282 four-noded axisyimmetric elements type CAX4R. The mesh near the contact was refined to improve the accuracy and convergence of the analysis and the mesh became gradually coarser when moving away from the initial contact region. The elements located along the contact were squares with sides 30 nm long. For each finite element simulation, the minimum number of elements in contact with the indenter at the maximum load was 30. Regarding the boundary conditions, nodes at the axis of symmetry were allowed to move only in the vertical direction and nodes at the bottom were fixed. In all finite element computations, the contact was modeled considering two surfaces with isotropic friction; contact that follows the model of Coulomb,[38] with friction coefficient equal to 0.15.[35] The specimen was modeled as a homogeneous and isotropic solid. The elastic and plastic behaviors of the indented material followed Hooke's law and hardening

power law, respectively, as indicated in Eq. (14). In all simulations, the large deformation formulation was considered

$$\sigma = \begin{cases} E\epsilon \ for \ \sigma \leq Y \\ K\epsilon^n \ for \ \sigma > Y \end{cases} \quad . \tag{14}$$

A total of 64 different finite element simulations were conducted controlling the indentation depth.

Note that the numerical model selected in this work presents differences with respect to the analytical models available in the literature, such as those provided by Hertz, Love, and Sneddon. For example, one can mention the consideration of plasticity, a friction coefficient at the indenter-specimen contact, and the use of large deformation analysis.

VI. EXPERIMENTAL PROCEDURE

Instrumented indentation tests were conducted in a Fischerscope H100V equipment manufactured by Helmut Fischer GmbH (Sindelfingen-Maichingen, Germany), equipped with a Vickers diamond indenter with a tip radius of approximately 1.33 μm.[39] Loads of 40, 50, 60, and 70 mN were applied during the tests.

The loading/unloading cycle consisted of an initial loading stage, followed by a holding stage of 30 s at the peak load with the aim of reducing creep effects. A holding time of 30 s was also applied at the end of the unloading stage to evaluate thermal drift effects. In each loading/unloading cycle, 200 data points were acquired in steps of 0.1 s at constant loading rate. At least 15 indentation tests were conducted in each specimen for each value of peak load and only those curves within two standard deviations from the average P_m/S^2_u ratio were used in the analysis of indentation data.[39]

When true replicates are made under a given set of experimental conditions, the variation between their associated observations may be used to estimate the standard deviation of a single experimental condition. In this case, the statistical significance of the effects may be judged from an estimate of variance obtained by genuine replication.[12] On the other hand, in computational analysis, such as those in finite element simulations, genuine replications do not provide a measure of experimental noise, hence the interactions between factors is generally assumed as a measure of error for the cases where the relationship between factor and response is linear.[40] In other words, if the model that describes the response as a function of the factors is linear, interactions between factors (second order terms not included in the model) are assumed as a measure of experimental error. In this work, the factors analyzed do not have a linear behavior, and the interaction effects between factors are expected to be significant in the analysis. For this reason, in the cases where an experimental measurement was possible the error was calculated from experimental tests and not from higher order interactions.

Usually, in experimental analyses, genuine replications are not made for all test conditions. In these cases, repetitions can be performed for a single set of experimental parameters, usually a central point, which may also be used to compare the effect magnitudes.[12] Using the same idea, in this work a confidence interval estimate was calculated by genuine replications in experimental trials using two different materials, whose mechanical properties are contained in the range covered by the 2^6 factorial design.

The materials used in the experimental error calculation were a low-carbon steel AISI 1006 and a high-carbon steel AISI 1080. The mechanical properties of these materials are shown in Table III, where E, Y, and n correspond to the average of the values taken from three repetitions of uniaxial tensile tests. All specimens were mechanically polished and finished until 0.025 μm with colloidal silica, aiming to obtain a good surface finish. It is well known that one of the most crucial parameters affecting the accuracy of the instrumented indentation results is the surface roughness.[41]

The confidence interval for the response variables was calculated using Eq. (15), where t is the probability of the t distribution with u degrees of freedom and s is the pooled estimate of run variance, Eq. (16).[12]

$$\delta = \pm t_u s \sqrt{\frac{1}{r_1} + \frac{1}{r_2} + \ldots + \frac{1}{r_g}} \quad , \tag{15}$$

$$s^2 = \frac{u_1 s_1 + u_2 s_2^2 + \ldots u_g s_g^2}{u_1 + u_2 + \ldots + u_g} \quad . \tag{16}$$

In Eqs. (15) and (16), g is the number of experimental conditions [8 = 2 (materials) ×4 (load levels)]; $u_i = r_i - 1$ provides the degrees of freedom of each experimental condition; r_i is the replicate run conducted at the ith set of experimental conditions and $u = u_{1+}u_{2+\ldots}u_g$ represents the degrees of freedom [123 = 131 (total indentation curves) − 8 (experimental conditions)]. Table IV shows the confidence interval with a 95% confidence level for the dimensionless functions that can be calculated directly from IIT curves (α, Π_1, Π_4, Π_6, Π_7). The dimensionless functions Π_2, Π_3, and Π_5 are not presented because the indentation area and level of pile-up or sink-in could not be measured directly.

TABLE III. Mechanical properties of the materials.

Material	E (GPa)	Y (MPa)	n
AISI 1006	200	221	0.200
AISI 1080	213	302	0.170

TABLE IV. Confidence interval.

Load	α	$\Pi_1 = P_l/Eh^2$	$\Pi_4 = S/Eh_{max}$	$\Pi_6 = h_{max}/h_f$	$\Pi_7 = W_p/WT$
40–70 mN	±0.0815	±0.0124	±0.3169	±0.0147	±0.0045
3 N[a]		±0.01934	±0.2439		±0.0084
10 N[b]		±0.0070	±0.1431	±0.0028	

[a]Confidence intervals for the test presented in Ref. 8 $N = 6$, $u = 10$, $g = 2$ (Al 6061 and Al 7075).
[b]Confidence intervals for the test presented in Ref. 42 $N = 6$, $u = 5$, $g = 1$ (Al 2098-T8).

TABLE V. Percent of variation caused by experimental error.

Load	α	$\Pi_1 = P_l/Eh^2$	$\Pi_4 = S/Eh_{max}$	$\Pi = h_{max}/h$	$\Pi_7 = W_p/WT$
40–70 mN	4.48%	2.58%	4.53%	1.3%	0.5%
3 N[a]		4.03%	3.48%		0.93%
10 N[b]		1.46%	2.04%	0.25%	

[a]For the test presented in Ref. 8 $N = 6$, $u = 10$, $g = 2$ (Al 6061 and Al 7075).
[b]For the test presented in Ref. 42 $N = 6$, $u = 5$, $g = 1$ (Al 2098-T8).

Table V presents the experimental error in percentage of the mean value of the response variable. Note that the $\Pi_4 = S/Eh_{max}$ confidence interval is the widest (Table IV) and the largest percentage of the average value (Table V), similar to the results calculated using the data presented in Refs. 8 and 42. This indicates that the initial unloading slope (S) is the test variable most susceptible to experimental errors. Additionally, when comparing the values obtained for the confidence interval of dimensionless function Π_4 with those calculated from the data in the literature,[8,42] it is possible to note that a decrease in the maximum load results in an increase in the confidence interval, which is not observed for the confidence interval of the dimensionless function Π_1.

VII. RESULTS AND DISCUSSION

Figures 3 and 4 present the overall effect of both dimensional and dimensionless factors on α and functions Π_1 to Π_7. Each point in these plots represents an average of all results calculated considering a given level of the factor. Besides, each plot presents a reference line that indicates the overall average value of the response represented in the plot, for all the 64 simulations that were conducted. The results from all simulations were also used to calculate the range of variation (effect l_i) in each plot. These results are presented in Table VI and those larger than the confidence interval (Table IV) were underlined. Table VI also presents the interaction effects (l_{ixj}).[12]

A. Exponent of the penetration depth in the load stage α

Similar to Rodríguez et al.,[22] Table VI indicates that the exponent α was significantly dependent of the ratio R/h_{max} and independent of the mechanical properties of

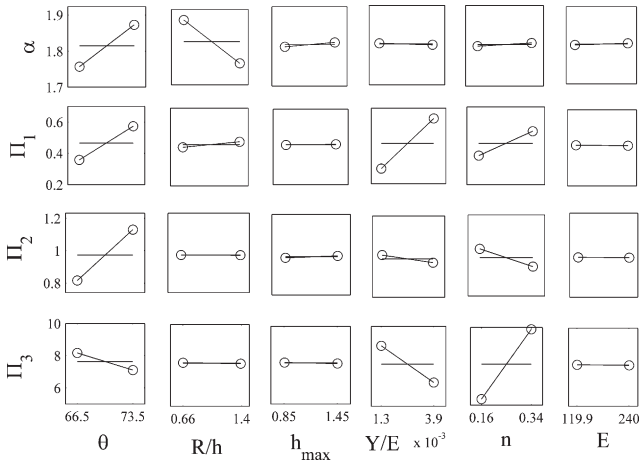

FIG. 3. Main effects plot (data means) for α, $\Pi_1 = P_l/Eh^2$, $\Pi_2 = h_c/h$, $\Pi_3 = H/Y$.

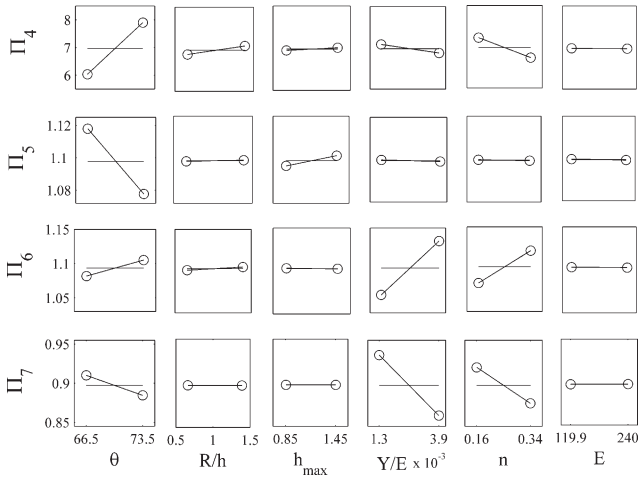

FIG. 4. Main effects plot (data means) for $\Pi_4 = S/Eh_{max}$, $\Pi_5 = \beta$, $\Pi_6 = h_{max}/h_f$, $\Pi_7 = W_p/W_T$.

TABLE VI. Main effects and interactions.

Effects	α	$\Pi_1 = P_l/Eh^2$	$\Pi_2 = h_c/h$	$\Pi_3 = H/Y$	$\Pi_4 = S/Eh_{max}$	$\Pi_5 = \beta$	$\Pi_6 = h_{max}/h_f$	$\Pi_7 = W_p/W_T$
$l_{Y/E}$	−0.0044	0.3318	−0.0455	−2.2980	−0.3190	−0.0012	0.0762	−0.0773
l_n	0.0087	0.1570	−0.1074	4.4895	−0.7553	−0.0034	0.0459	−0.0460
$l_{R/h}$	−0.1150	0.0356	−0.0015	−0.0558	0.3017	0.0000	0.0045	−0.0002
l_θ	0.1160	0.2150	0.3145	−1.0644	1.8805	−0.0427	0.0234	−0.0255
l_E	0.0048	−0.0027	−0.0016	−0.0319	−0.0133	−0.0005	−0.0006	0.0002
l_h	0.0122	0.0041	0.0115	−0.0605	0.0912	0.0053	−0.0007	−0.0000
$l_{Y/E\times n}$	−0.0045	0.0197	0.0018	−1.3076	0.0227	0.0018	0.0123	−0.0094
$l_{Y/E\times R/h}$	−0.0043	0.0074	−0.0103	0.0445	−0.0681	0.0006	0.0017	0.0006
$l_{Y/E\times\theta}$	0.0062	0.0720	−0.0123	0.1028	−0.0898	−0.0017	0.0099	−0.0092
$l_{Y/E\times E}$	−0.0033	−0.0061	−0.0095	0.0493	−0.0493	0.0029	−0.0006	0.0009
$l_{Y/E\times h}$	−0.0037	0.0022	0.0039	0.0080	0.0135	−0.0022	−0.0012	0.0000
$l_{n\times R/h}$	0.0051	0.0128	0.0087	−0.0801	0.0301	−0.0050	0.0030	−0.0009
$l_{n\times\theta}$	−0.0064	0.0278	−0.0117	−0.5708	−0.0718	−0.0004	0.0032	−0.0028
$l_{n\times E}$	0.0038	0.0062	0.0097	−0.0483	0.0533	−0.0023	0.0007	−0.0008
$l_{n\times h}$	0.0047	−0.0028	−0.0012	−0.0353	−0.0122	−0.0002	−0.0007	0.0004
$l_{R/h\times\theta}$	0.0276	−0.0011	−0.0061	0.0297	−0.0507	−0.0004	−0.0008	0.0001
$l_{R/h\times E}$	0.0040	0.0062	0.0097	−0.0484	0.0527	−0.0024	0.0008	−0.0008
$l_{R/h\times h}$	−0.0013	−0.0015	−0.0026	−0.0197	−0.0044	−0.0002	−0.0011	0.0003
$l_{\theta\times E}$	−0.0049	0.0026	0.0016	0.0313	0.0137	0.0005	0.0005	−0.0002
$l_{\theta\times h}$	−0.0069	−0.0058	−0.0078	0.0325	−0.0304	0.0026	−0.0012	0.0010

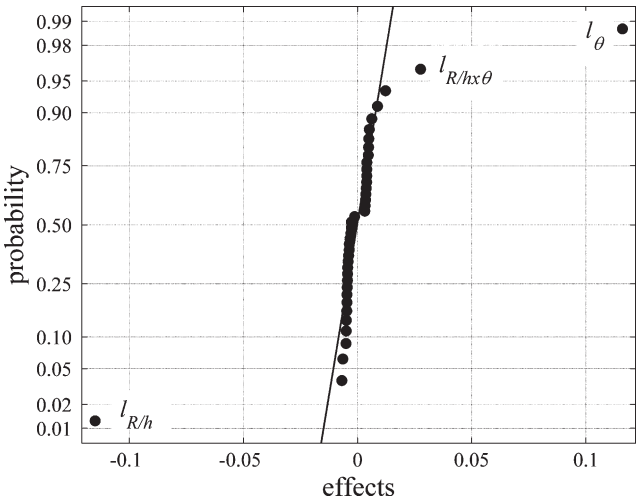

FIG. 5. Normal plot of effects for α. The figure presents 40 data points corresponding to effects from first to third order. The effects outside the straight line are statistically significant.

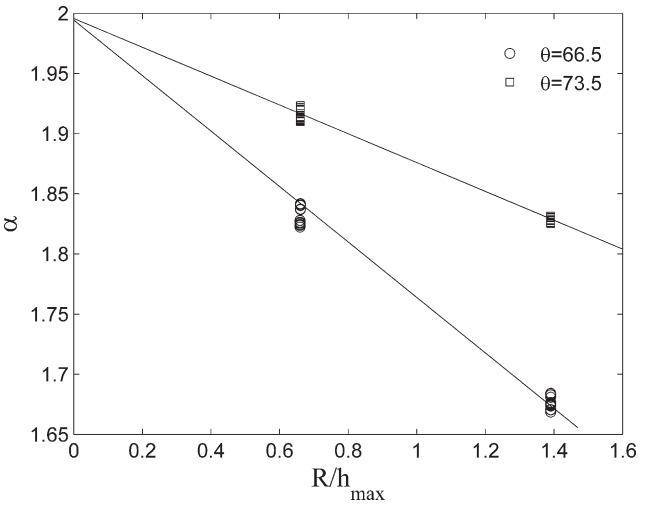

FIG. 6. Loading curve α as a function of tip roundness for different indenter angles. Each datum corresponds to a test condition in the factorial design.

the indented material. Table VI also indicates that α was significantly dependent of θ. The significant effect of R/h_{max} and θ on α can also be visually seen in Fig. 3. This figure indicates that at the levels studied in this work, the exponent α increases when θ increases and decreases when the ratio R/h_{max} increases.

In terms of the interaction factors, Table VI shows that the value of $l_{R/h\times\theta}$ was lower than the confidence interval for α, which would indicate that the combined effect of R/h_{max} and θ was not significant. However, when the effects are plotted on normal probability paper (Fig. 5), where significant effects appear displaced with respect to the straight line,[12] the interaction effect between R/h_{max} and θ is not on the straight line and may not be explained as a product of error. The elastic contact theory states that the exponent α is 2 for the contact between a cone and a flat surface, independent of θ.[23] This literature result, obtained for a cone without tip roundness, is not contrary to the results presented in Figs. 3 and 5, even considering that the results in these figures indicate that the exponent α is significantly affected by θ. The agreement between literature and numerical results is clear when values of α are plotted as a function of R/h_{max} (Fig. 6). An extrapolation of the values of α (for each angle θ) to R/h_{max} equal to zero provides α approximately equal to 2, as predicted by the elastic contact theory. However, when R/h_{max} is different from zero, the variation of α with R/h_{max} presents

different slopes, depending on θ. The effect l_θ plotted in Fig. 5 is a measure of the difference in α caused by changing θ in each level of R/h_{max} shown in Fig. 6.

That change in α with θ is due to the combined effect of both R/h_{max} and θ ($l_{R/h\times\theta}$). This fact is in agreement with the statistical effect analysis,[12] in which the main effect of a factor should be individually interpreted only if there is no evidence that the factor interacts with other factor. This precaution is particularly important for algorithms based on indentation curves obtained with different sharp indenters, because it might indicate that conclusions of evaluations of tip roundness effects for a specific indenter angle cannot be extrapolated for indenters with other angles.

B. Load dimensionless function in the loading stage

Figure 3 shows the main effects for the dimensionless function $\Pi_1 = P_l/Eh^2$. Significant effects on function Π_1 were found for all the dimensionless factors (Y/E, R/h_{max}, and n) analyzed in this work. However, no significant dependence was found for the dimensional factors (E, h_{max}). These results indicate that an identical loading curve was obtained considering different E values, but the same Y/E ratio. Similarly, an identical loading curve was obtained for different h_{max}, but with the same R/h_{max} level.

Figure 3 shows that as reported in Refs. 10 and 11, Π_1 increases when Y/E, θ, R/h_{max}, and n increase. Furthermore, as reported in Refs. 4 and 22 the ratio R/h_{max} has little but not negligible effect. All effects larger than the confidence interval (Table VI) may also be visualized in the normal plot of effects (Fig. 7), as points not located on the straight line. The interaction observed for R/h_{max} and n suggests that assessments on the influence of indenter tip defects should not be extrapolated to the analysis of the indentation of materials with different mechanical properties without regarding this combined effect between indenter roundness parameter and hardening exponent.

C. Pile-up or sink-in behavior

Figure 3 shows the main effects for the dimensionless function $\Pi_2 = h_c/h$. Significant effects on function Π_2 were found for the dimensionless factors Y/E, θ, and n and no significant dependence was found for the dimensional factors (E, h_{max}). As reported in Ref. 6, Π_2 increases when Y/E and n decrease and increases when θ increases. For the conditions evaluated in this work, the ratio R/h_{max} showed a negligible effect. Figure 8 shows the normal plot of effects for Π_2, which includes the combined effects of two and three factors. In this case, only the isolated effects of Y/E, n, and θ have shown evident separation from the straight line and, thus, significant values.

D. Hardness

Figure 3 shows the main effects for the dimensionless function $\Pi_3 = H/Y$. Significant effects on this function were found for the dimensionless factors Y/E, θ, and n and no significant dependence was found for the dimensional factors (E, h_{max}). As reported in Ref. 11, Π_3 decreases when Y/E increases and increases when n increases. As reported in Ref. 43, considering the range of values of θ analyzed in this work, the function Π_3 decreases when θ increases. For the conditions evaluated in this work the ratio R/h_{max} showed a negligible effect, in accordance with Ref. 22. Similar to the previous functions, Fig. 9 presents the most significant effects, where it is possible to see that the second order interactions ($l_{Y/E\times n}$ and $l_{\theta\times n}$) may not be neglected.

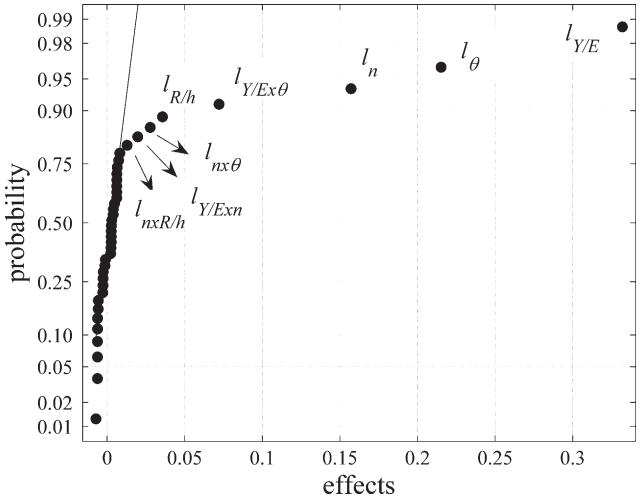

FIG. 7. Normal plot of effects for $\Pi_1 = P_l/Eh^2$.

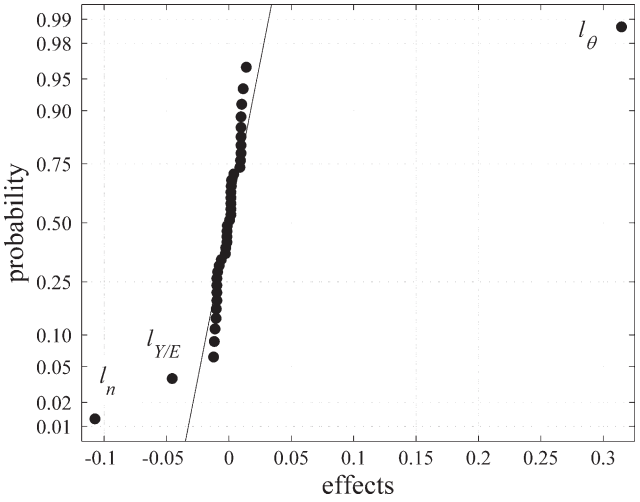

FIG. 8. Normal plot of effects for $\Pi_2 = h_c/h$.

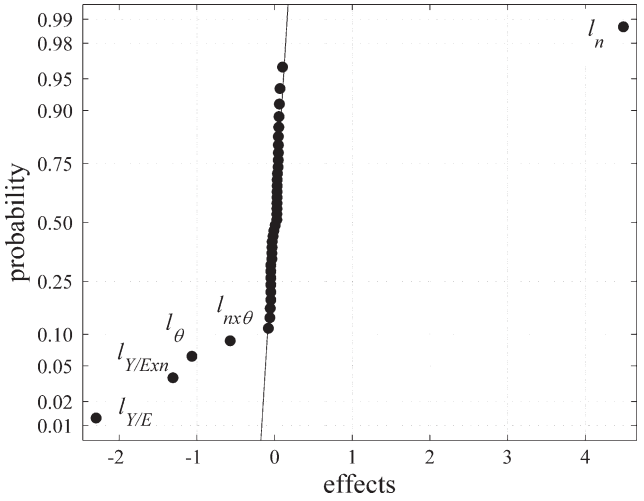

FIG. 9. Normal plot of effects for $\Pi_3 = H/Y$.

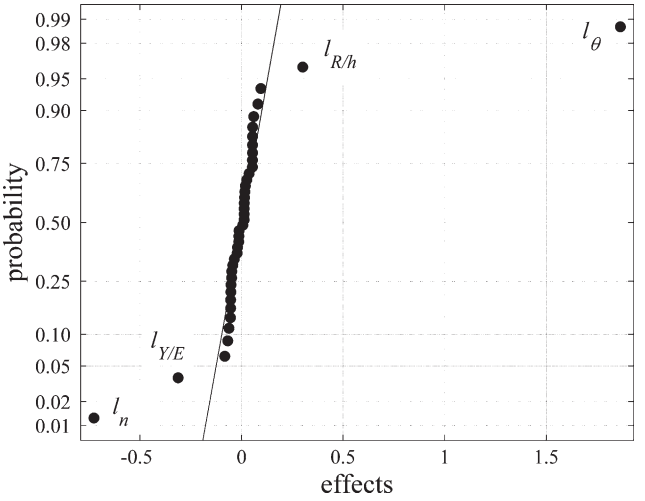

FIG. 11. Normal plot of effects for $\Pi_4 = S/Eh_{max}$.

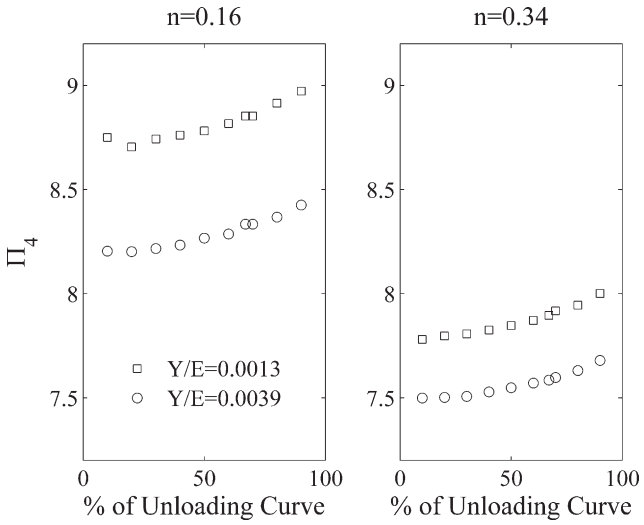

FIG. 10. $\Pi_4 = S/Eh_{max}$ evolution with the percentage of the unloading curve considered in the fit of the points of the unloading curve, $R/h_{max} = 1.354$, $h_{max} = 1.453$ (μm), $E = 119.93$ (GPa) $\theta = 73.5°$.

E. Initial unloading slope

All simulated unload curves were fitted to Eq. (2) using a different percentage of unloading curve data. As suggested by Eq. (2), the variables used in the fit were K, m, and h_f and, in all cases, the minimum value of r^2 was 0.999965 and at least 10 points were taken in each fit of unloading data. The initial unloading slope S was calculated as the derivative with respect to the indenter displacement [Eq. (2)] using K, m, and h_f from fitted unloading data. Results indicate that the initial unloading slope was dependent of the fitted percentage of unloading curve data, as presented in Fig. 10, which shows the results for four combinations of mechanical properties.

Variation of S with the fitted percentage of the unloading data was also reported in Ref. 31 where the estimated value of the initial unloading slope stabilized when the fraction of data considered was between 60% and 90%.

To quantify the intensity of the effect of the fraction of unloading curve data, two levels were established for that factor: 40% as a low level and 70% as a high level. In this case, the calculated effect value was $l_{\%} = 0.07399$; a magnitude lower than the confidence interval from the experimental error in any load level (Tables IV–VI).

Figure 4 shows the main effects for the dimensionless function $\Pi_4 = S/Eh_{max}$. Significant effects on this function were found for all the dimensionless factors and no significant dependence was found for the dimensional factors (E, h_{max}). As reported in Ref. 11, Π_4 decreases when Y/E and n increase. The function Π_4 increases when θ increases. According to Ref. 22 the ratio R/h_{max} has a little but not negligible effect. Figure 11 shows the normal plot of effects for Π_4, where it is possible to see that the combined effects were not significant in this case.

F. Correction factor of the Sneddon's equation

Once a significant variation of S was found with respect to the percentage of data used in the fitting of the unloading curve, it seems appropriate to analyze the dependence of the correction factor β from this factor. Figure 12 shows the variation of β as a function of the percentage of the data considered in the fit of the unloading curve; for four combinations of mechanical properties. In Fig. 12, one can note that the variation of β with the percentage of the curve fit is higher than the variation caused by either n or Y/E. This result implies that an experimental analysis on the variation of β should be difficult to implement, because the experimental error of S is large. Furthermore, in this type of analysis results are additionally affected by the experimental error in

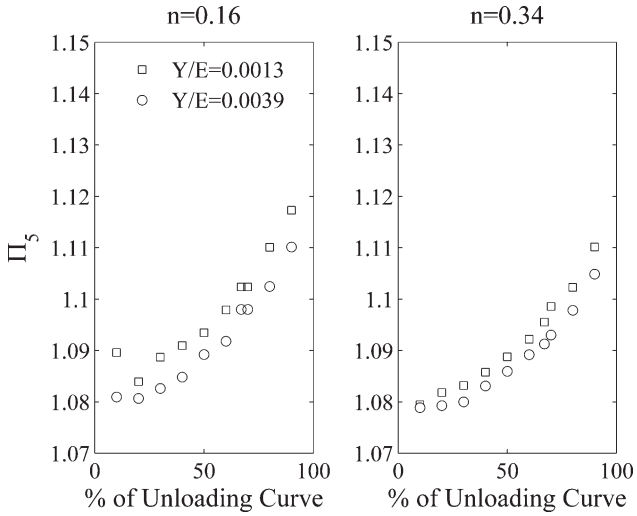

FIG. 12. $\Pi_5 = \beta$ evolution with the percentage of the unloading curve considered in the fit of the points of the unloading curve, R/h_{max} = 1.354, h_{max} = 1.453 (μm), E = 119.93 (GPa) θ = 73.5°.

contact area measurement, which is either based on the analysis of the residual imprint or on an indirect measurement, such as that proposed by the Oliver and Pharr method.[25]

According to Cheng,[11] the correction factor β is roughly independent of Y/E and n and for θ = 68°, and ν = 0.3 has a value equal to 1.085 ± 0.025. This work provides further confirmation that β is independent of Y/E and E; yet n has shown little effect (Table VI), which was also observed by Bolshakov.[44] Table VI indicates that the effect of the strain hardening exponent (n) (−0.0034) is comparable to the effect caused by the indentation size h_{max} (0.0053). In the literature, it has been suggested that the effect of the indentation size is caused by tip roundness effects[5,32,33]; yet the effect caused by the ratio R/h_{max} reported in Refs. 5, 32, and 33 was obtained by an increment of h_{max} while maintaining a constant radius. On the other hand, when the ratio R/h_{max} was evaluated by changing the radius and maintaining the h_{max} constant[22] a tendency for change in β was not observed.

As presented in Ref. 28, Fig. 4 shows that the indenter angle has an important effect on β and that when θ increases, β decreases. Furthermore, two analyses were conducted in terms of the normal plot of effects related to the factor β (Fig. 13). The first one, Fig. 13(a), was conducted considering a fixed value for the percent of data selected to fit the unloading curve. In this case, with the exception of the effect caused by the angle of the indenter, all effects are so small that they are not distinguishable from experimental errors. On the other hand, when the fraction of the unload curve is incorporated as a factor, a better estimate of the error is obtained, because the normal probability plot incorporates the effects

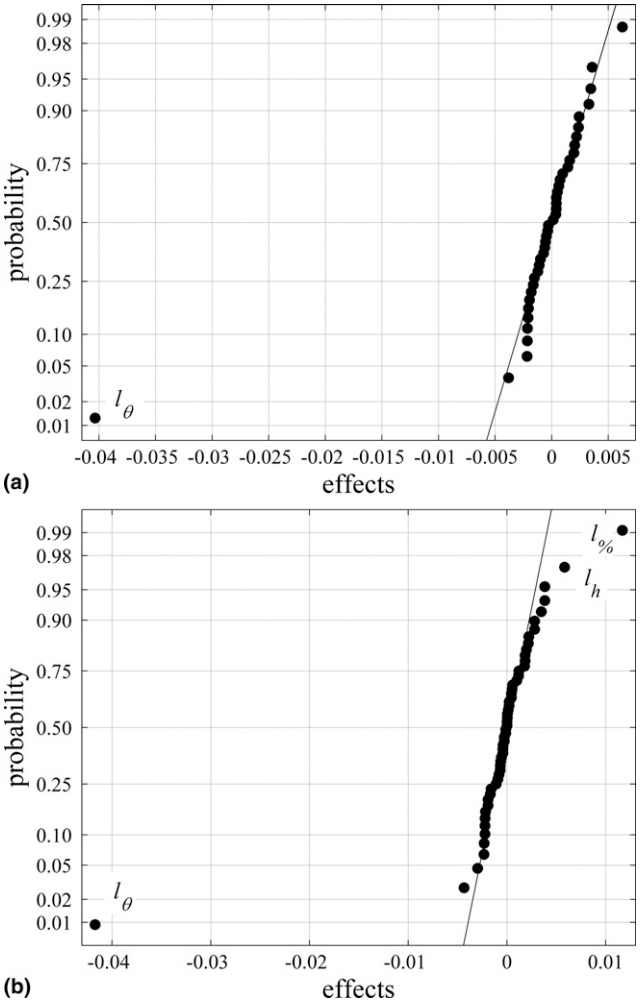

FIG. 13. Normal plot of effects for $\Pi_5 = \beta$ (a) 67% percentage of the unloading curve considered, (b) factor percentage of the unloading curve at two levels.

of additional factors. In this case, the fraction used to fit the unloading data and the maximum depth of indentation appears as significant [Fig. 13(b)].

G. Dimensionless function $\Pi_6 = h_{max}/h_f$

To analyze the dimensionless function $\Pi_6 = h_{max}/h_f$, the residual indentation depth h_f was taken directly from the end of the unload simulation curve and not from the fit of the unloading curve. This selection avoided the effect of the percentage of data used in the fitting of the unloading curve. Although function Π_6 depends on the dimensionless variable R/h_f [Eq. (12)], R/h_f cannot be used as a factor in the factorial design of experiments because its value cannot be fixed as an input parameter for the simulations. Figure 4 shows the main effects for the dimensionless function Π_6. Significant effects on this function were found for all the dimensionless factors and no significant dependence was found for the dimensional factors (E, h_{max}). Figure 4 shows that

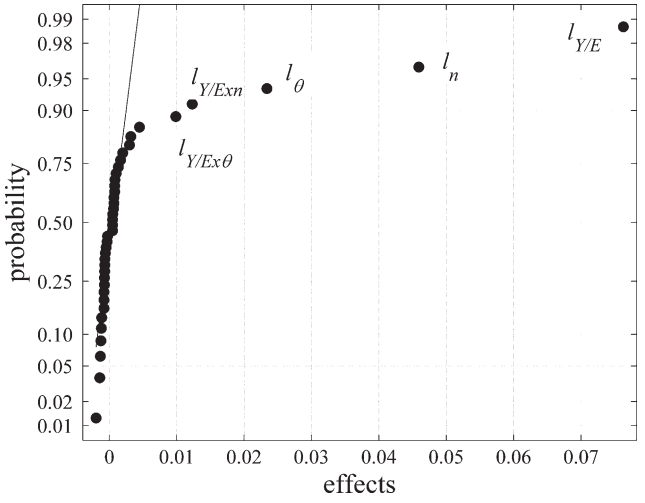

FIG. 14. Normal plot of effects for $\Pi_6 = h_{max}/h_f$.

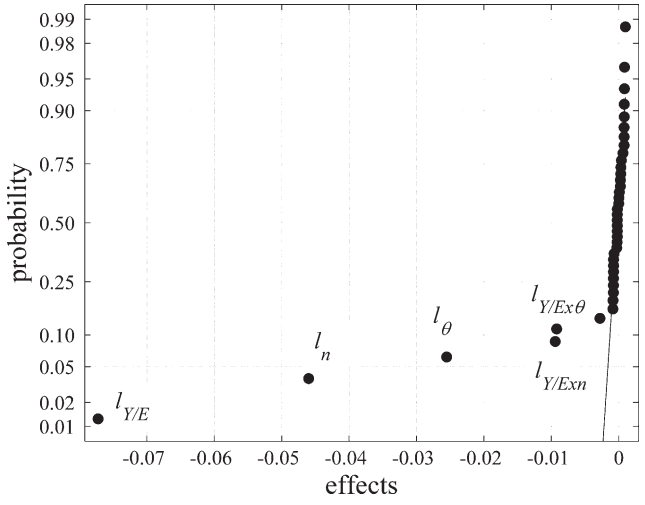

FIG. 15. Normal plot of effects for $\Pi_7 = W_p/W_T$.

Π_6 increases when Y/E, n, θ, and R/h_{max} increase. As reported in Ref. 22, the ratio R/h_{max} has little effect on Π_6 for the range of Y/E values analyzed in this work. The effect of R/h_{max} cannot be differentiated from experimental error (Table IV) and fall on the straight line of the normal plot (Fig. 14).

H. Dimensionless function $\Pi_7 = W_p/W_T$

Figure 4 shows the main effects for the dimensionless function $\Pi_7 = W_p/W_T$. Significant effects on this function were found for the dimensionless factors Y/E, θ, and n and no significant dependence was found for the dimensional factors (E, h_{max}). As reported by Cheng,[7] Π_7 decreases when Y/E and n increase. Additionally, Fig. 4 shows that Π_7 decreases when θ increases. As reported in Ref. 22 for the conditions evaluated in this work, the ratio R/h_{max} showed a negligible effect. Figure 15 shows the normal plot of effects for Π_7. As previously, the effects underlined in the Table VI, which are larger than the confidence interval for function Π_7, were the same that showed a significant effect in the normal plot, characterized by deviations from the straight line.

VIII. CONCLUSIONS

In this work, a few finite element simulations allowed the identification of the effects of some variables on the indentation response of elastic–plastic materials under conical indentation. These variables were associated with the mechanical properties of the indented material, as well as with the indenter geometry. Using dimensional analysis, it was possible to select dimensionless functions that describe the load during loading stage, the depth of contact, the initial unloading slope, the residual depth, and the ratio between plastic and total indentation work. Furthermore, the dimensionless variables that describe these functions were also defined.

The influence of indenter tip roundness ($0.67 < R/h_{max} < 1.4$) on the characteristics of the instrumented indentation curve was quantified. The dimensionless functions $\Pi_1 = P_l/Eh^2$ and $\Pi_4 = S/Eh_{max}$ and the exponent of loading stage α were strongly influenced by the ratio R/h_{max}. However, no effect of this variable was found for the ratios H/Y, W_p/W_T, and h_{max}/h_f.

This work has also confirmed that β is not well described by dimensional analysis. It was also possible to observe that β is independent of the mechanical properties of the indented material analyzed in this work (Y, E, and n), although little effect was found for the hardening exponent n. No dependence of β was found with respect to the ratio R/h_{max} in the range studied for this variable ($0.67 < R/h_{max} < 1.4$); yet β showed a dependence with the maximum indentation depth. Excluding the effect caused by the angle of the indenter, all effects on β were small, such that they would be hardly distinguishable from experimental error. However, β showed a strong dependence of the fraction of data used to fit the unloading curve, which indicates that β is especially susceptible to errors in the calculation of the initial unloading slope.

Although it is not entirely safe to extrapolate the effects presented in this work outside the range selected for the input variables, the procedure presented in the previous sections can be implemented in the first stages of indentation studies for mechanical properties calculation, minimizing the time required for simulations. The factors that present a significant effect should be compared with the confidence interval of the experimental results, or normal plots should be used to determine which factors can or cannot be excluded from the analysis, which also includes an evaluation of combined effects from the input variables.

ACKNOWLEDGMENTS

This research was sponsored by The National Council for Scientific and Technological Development (CNPq) under Contract No. 141259/2007-8 and by The State of Sao Paulo Research Foundation (FAPESP).

REFERENCES

1. *Instrumented Indentation Testing,* 10th ed., ASM Handbook, Vol. 8**,** edited by J.L. Hay and G.M. Pharr (ASM, Materials Park, OH, 1990), pp. 232–243.
2. X. Li and B. Bhushan: A review of nanoindentation continuous stiffness measurement technique and its applications. *Mater. Charact.* **48,** 11 (2002).
3. A.C. Fischer-Cripps: A review of analysis methods for sub-micron indentation testing. *Vacuum* **58,** 569 (2000).
4. Y.T. Cheng and C.M. Cheng: Further analysis of indentation loading curves: Effects of tip rounding on mechanical property measurements. *J. Mater. Res.* **13,** 1059 (1998).
5. J.M. Meza, F. Abbes, and M. Troyon: Penetration depth and tip radius dependence on the correction factor in nanoindentation measurements. *J. Mater. Res.* **23,** 725 (2008).
6. Y.T. Cheng and C.M. Cheng: Effects of "sinking in" and "piling up" on estimating the contact area under load in indentation. Philos. *Mag. Lett.* **78,** 115 (1998).
7. Y.T. Cheng and C.M. Cheng: Relationships between hardness, elastic modulus, and the work of indentation. *Appl. Phys. Lett.* **73,** 614 (1998).
8. M. Dao, N. Chollacoop, K.J. Van Vliet, T.A. Venkatesh, and S. Suresh: Computational modeling of the forward and reverse problems in instrumented sharp indentation. *Acta Mater.* **49,** 3899 (2001).
9. J.L. Bucaille, S. Stauss, E. Felder, and J. Michler: Determination of plastic properties of metals by instrumented indentation using different sharp indenters. *Acta Mater.* **51,** 1663 (2003).
10. Y.T. Cheng and C.M. Cheng: Scaling, dimensional analysis, and indentation measurements Mater. *Mater. Sci. Eng., R* **44**, 91 (2004).
11. Y.T. Cheng and C.M. Cheng: Scaling approach to conical indentation in elastic-plastic solids with work hardening. *J. Appl. Phys.* **84,** 1284 (1998).
12. G.E.P. Box, W.G. Hunter, and J.S. Hunter: *Statistics for Experimenters. An Introduction to Design, Data Analysis, and Model Building*. 1st ed. (John Wiley, New York, 1978), pp. 117–434.
13. C. Bisch, M. Nadal, F. Teyssandier, M. Bancel, and B. Vallon: Chemical vapor deposition of titanium carbide on WC-Co cemented carbides. *Mater. Sci. Eng., A* **202,** 238 (1995).
14. J.R. Correa, D. Canetti, R. Castillo, J.C. Llópiz, and J. Dufour: Influence of the precipitation pH of magnetite in the oxidation process to maghemite. *Mater. Res. Bull.* **41,** 703 (2006).
15. R.L. Perrier, A. Safari, and R.E. Riman: Experimental design applied to a low-temperature synthetic route to crystalline, submicron barium titanate zirconate powder. *Mater. Res. Bull.* **26,** 1067 (1991).
16. M.C.M. Farias, R.M. Souza, A. Sinatora, and D.K. Tanaka: The influence of applied load, sliding velocity and martensitic transformation on the unlubricated sliding wear of austenitic stainless steels. *Wear* **263,** 773 (2007).
17. L.M. Moore, M.D. McKay, and K.S. Campbell: Combined array experiment design. *Reliab. Eng. Sys. Safety* **91,** 1281 (2006).
18. M. Calì, M.G.L. Santarelli, and P. Leone: Computer experimental analysis of the CHP performance of a 100 kWe SOFC field unit by a factorial design. *J. Power Sources* **156,** 400 (2006).
19. N. Jakobsson, D. Karlsson, J.P. Axelsson, G. Zacchi, and B. Nilsson: Using computer simulation to assist in the robustness analysis of an ion-exchange chromatography step. *J. Chromatogr., A* **1063,** 99 (2005).
20. X. Wang and G.A. Dumas: Evaluation of effects of selected factors on inter-vertebral fusion—A simulation study. *Med. Eng. Phys.* **27,** 197 (2005).
21. O. Casals and J. Alcalá: Analytical and experimental resolutions in the duality of mechanical property extractions from instrumented indentation experiments: Comments on "On determination of material parameters from loading and unloading responses in nanoindentation with a single sharp indenter" by L. Wang and S.I. Rokhlin. [*J. Mater. Res.* **21,** 995 (2006)]. *J. Mater. Res.* **22,** 1138 (2007).
22. S.A. Rodriguez, M.C.M. Farias, and R.M. Souza: Analysis of the tip roundness effects on the micro and macroindentation response of elastic-plastic materials. *J. Mater. Res.* **24,** (2009, DOI: 10.1557/JMR.2009.0078).
23. I.N. Sneddon: The relationship between load and penetration in the axisimetric Boussinesq problem for a punch of arbitrary profile. *Int. J. Eng. Sci.* **3,** 47 (1965).
24. H. Hertz and J.R. Angew: On the contact of elastic solids. *Math.* **92,** 156 (1881) (Translated and reprinted in English in *Hertz's Miscellaneous Papers*, Macmillan, London, 1896).
25. W.C. Oliver and G.M. Pharr: An improved technique for determining hardness and elastic modulus using load and sensing indentation experiments. *J. Mater. Res.* **7,** 1564 (1992).
26. M. Martin and M. Troyon: Fundamental relations used in nanoindentation: Critical examination based on experimental measurements. *J. Mater. Res.* **17,** 2227 (2002).
27. R.B. King: Elastic analysis of some punch problems for a layered medium. *Int. J. Solids Struct.* **23,** 1657 (1987).
28. J.C. Hay, A. Bolshakov, and G.M. Pharr: A critical examination of the fundamental relations used in the analysis of nanoindentation data. *J. Mater. Res.* **14,** 2296 (1999).
29. J.L. Hay and P.J. Wolff: Small correction required when applying the Hertzian contact model to instrumented indentation data. *J. Mater. Res.* **16,** 1280 (2001).
30. J.M. Meza and J. Cruz: Tip roundness effect in mechanical properties measured by instrumented indentation. *Sci. Teach.* **36,** 613 (2007).
31. J.M. Antunes, L.F. Menezes, and J.V. Fernandes: Three-dimensional numerical simulation of Vickers indentation tests. *Int. J. Solids Struct.* **43,** 784 (2006).
32. M. Troyon and L. Huang: Correction factor for contact area in nanoindentation measurements. *J. Mater. Res.* **20,** 610 (2005).
33. M. Troyon and S. Lafaye: About the importance of introducing a correction factor in the Sneddon relationship for nanoindentation measurements. *Philos. Mag.* **86,** 5299 (2006).
34. Y.P. Cao, M. Dao, and J. Lu: A precise correcting method for the study of the superhard material using nanoindentation tests. *J. Mater. Res.* **22,** 1255 (2007).
35. M. Mata and J. Alcalá: The role of friction on sharp indentation. *J. Mech. Phys. Solids* **52,** 145 (2004).
36. S. Suresh and A.E. Giannakopoulos: A new method for estimating residual stresses by instrumented sharp indentation. *Acta Mater.* **46,** 5755 (1998).
37. A.C. Fischer-Cripps: Use of combined elastic modulus in depth-sensing indentation with a conical indenter. *J. Mater. Res.* **18,** 1943 (2003).

38. Theory Manual 5.1-1, ABAQUS, version 6.7.
39. J.M. Meza, M.C. Moré, R.M. Souza, and L.J. Cruz: Using the ratio: Maximum load over unload stiffness squared, P_m/S_u^2, on the evaluation of machine stiffness and area function of blunt indenters on depth-sensing indentation equipment. *Mater. Res.* **10,** 437 (2007).
40. J. Sacks, S.B. Schiller, and W.J. Welch: Designs for computer experiments. *Technometrics* **31,** 41 (1989).
41. K.D. Bouzakis, N. Michailidis, S. Hadjiyiannis, G. Skordaris, and G. Erkens: The effect of specimen roughness and indenter tip geometry on the determination accuracy of thin hard coatings stress–strain laws by nanoindentation. *Mater. Char.* **49,** 149 (2003).
42. O. Casals and J. Alcalá: The duality in mechanical property extractions from Vickers and Berkovich instrumented indentation experiments. *Acta Mater.* **53,** 3545 (2005).
43. Y.T. Cheng and Z. Li: Hardness obtained from conical indentations with various cone angles. *J. Mater. Res.* **15,** 2830 (2000).
44. A. Bolshakov and G.M. Pharr: Influences of pileup on the measurement of mechanical properties by load and depth-sensing indentation techniques. *J. Mater. Res.* **13,** 1049 (1998).